

GaitFM: Fine-grained Motion Representation for Gait Recognition

Lei Wang¹, Fangfang Liang¹, Bincheng Wang¹, and Bo Liu¹

Hebei Agricultural University, Baoding 071000, Hebei, China
{20212060107,20212060108}@pgs.hebau.edu.cn
{liangfangfang,boliu}@hebau.edu.cn

Abstract. Gait recognition aims at identifying individual-specific walking patterns, which is highly dependent on the observation of the different periodic movements of each body part. However, most existing methods treat each part equally and neglect the data redundancy due to the high sampling rate of gait sequences. In this work, we propose a fine-grained motion representation network (GaitFM) to improve gait recognition performance in three aspects. First, a fine-grained part sequence learning (FPSL) module is designed to explore part-independent spatio-temporal representations. Secondly, a frame-wise compression strategy, called local motion aggregation (LMA), is used to enhance motion variations. Finally, a weighted generalized mean pooling (WGeM) layer works to adaptively keep more discriminative information in the spatial downsampling. Experiments on two public datasets, CASIA-B and OUMVLP, show that our approach reaches state-of-the-art performances. On the CASIA-B dataset, our method achieves rank-1 accuracies of 98.0%, 95.7% and 87.9% for normal walking, walking with a bag and walking with a coat, respectively. On the OUMVLP dataset, our method achieved a rank-1 accuracy of 90.5%¹.

1 Introduction

Gait recognition has emerged as a promising biometric technology that leverages human gait information for long-distance identification without the cooperation of subjects, which has shown great potential in many fields including video surveillance [1], rail transit [2], and sports simulation [3]. However, the performance of gait recognition suffers from various factors in real-world scenarios, e.g., changing viewpoints [4,5], occlusion [6,7], and wearing conditions [8,9]. Therefore, learning gait representations invariant to these factors is a major challenge for gait recognition.

Benefiting from the advances in deep learning techniques, most existing methods utilize convolutional neural networks (CNN) to extract spatio-temporal information from gait data. In general, depending on whether the temporal order of frames is considered or not, gait recognition methods fall into two categories: set-based and sequence-based.

¹ The source code can be found in the supplementary materials.

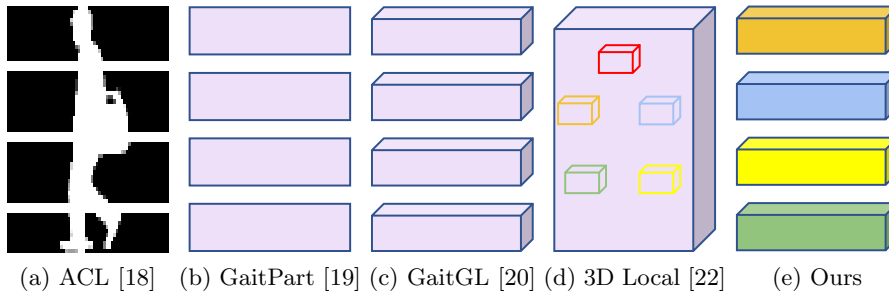


Fig. 1. Illustrations of different splitting strategies. We adopt the same strategy as GaitGL [20] but handle each part sequence independently.

The set-based methods treat a gait sequence as an unordered set, which either compress a set into a single gait template at the preprocessing stage [10,11], or learn order-independent gait representations from silhouette sets [12,13,14,15]. These methods assume that different subjects share a similar global walking pattern during a gait period, so the ordering of inputs is not essential for gait assessment. However, ignoring the temporal nature of the gait sequence could result in missing discriminative local motion information.

The sequence-based methods tend to explore individual gait patterns from multiple spatial and temporal scales [16,17,18,19,20,21,22]. As the input sequences are usually aligned, a uniform horizontal division of input images [18] or intermediate layer features [19,20,21] can improve recognition performance. Other approaches introduce a learnable partitioning strategy [23] or a body part-level localization module [22] to achieve a more adaptive local representation. Nevertheless, localization errors caused by changes in wear conditions or movement amplitude may degrade recognition accuracy. Fig. 1 illustrates different splitting strategies for gait silhouettes. Moreover, the redundancy of adjacent frames limits the recognition of spatio-temporal variation patterns. While some methods have been proposed to aggregate local clips [20,21,17], they also require extra parameter learning.

To address the above issues, we propose a novel fine-grained motion learning framework (GaitFM) for cross-view gait recognition. Specifically, GaitFM consists of three main components: a fine-grained part sequence learning (FPSL) module, a local motion aggregation (LMA) operation and a weighted generalized mean pooling (WGeM) layer. Instead of using shared convolutional kernels to extract part-specific features, in FPSL, the fine-grained motion patterns are independently obtained from body-part sequences (as shown in Fig. 1(e)). To reduce the redundancy of adjacent frames, the LMA compresses a sequence by aggregating information in each local clip. Additionally, the WGeM employs an attention mechanism to improve the spatial discriminability of feature maps. The contributions of our work are summarised as follows:

1. We propose a gait recognition framework named GaitFM, which combines global and fine-grained motion information for gait sequence learning.
2. We propose an LMA module to reduce the redundancy in the gait sequence and a WGeM pooling layer to selectively aggregate spatial information.
3. Experimental results on two public datasets, CASIA-B and OUMVLP, demonstrate that our method achieves state-of-the-art performance. Additional ablation studies verify the effectiveness of each module.

2 Related Work

According to order sensitivity, there are two main categories of gait recognition techniques: set-based and sequence-based.

2.1 Set-based Methods

In set-based approaches, gait silhouettes are typically considered as an unordered set, from which a set-level representation is obtained by characterizing the complementarity of the silhouettes in the set [10,12,13,14,24,15]. A straightforward way to handle a set of silhouettes is to compress them into a single template, i.e., gait energy image (GEI) [25], allowing the feature extraction and matching processes to be performed at the image level [10,11]. However, these template-based methods largely ignore the spatial and temporal properties during preprocessing. In order to maximally preserve the set information, some methods take the raw silhouettes as inputs [12,13,15]. Chao et al. [12] first propose a set-based gait recognition framework named GaitSet, which employs a max-pooling function to learn a permutation-invariant representation of a set. Hou et al. [13] further propose a lateral connection to fuse silhouette-level and set-level features. Additionally, the quality of each silhouette and part is evaluated to enhance the interpretability of the recognition model [15]. While the methods above provide flexibility through dropping the sequential constraints, the temporal cues are also essential for revealing subtle gait changes.

2.2 Sequence-based Methods

Sequence-based approaches emphasize continuous pose variations, aggregating multi-scale motion features associated with body models or silhouettes. The model-based methods extract geometric and dynamic gait features from human motion models, which have shown advantages in robustness to view and wearing changes [26,27,28]. However, these approaches suffer from performance degradation caused by the inaccurate pose estimation results from low-resolution conditions. The silhouette-based methods usually extract spatio-temporal gait information from the sequence [16,17,18,19,20,21,22]. To capture the various temporal cues in the sequence, some researchers considered extracting gait information from multiple temporal scales [16,17]. For example, Lin et al. [16]

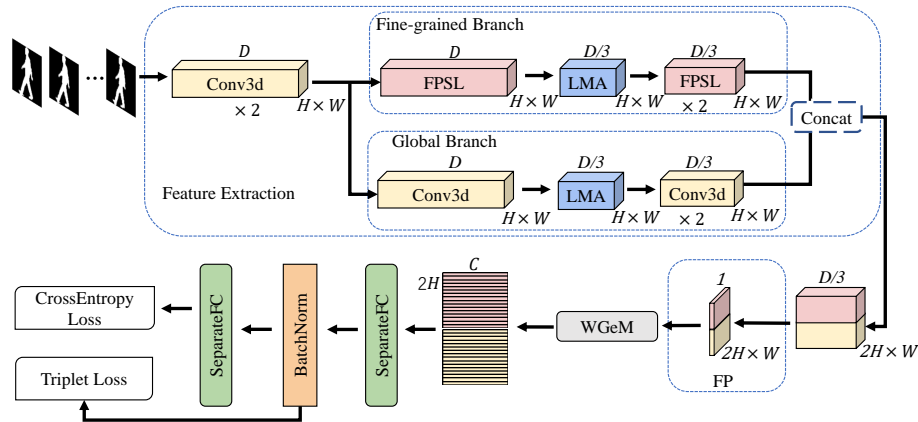


Fig. 2. Overview of GaitFM. The spatio-temporal dimensions of the feature map, i.e., D , H and W , are indicated in the figure, and we omit the channel dimension C for simplicity. There are two branches for motion feature extraction, both of which use the LMA module for sequence compression. The main difference is that the local branch employs the FPSL module to obtain part-based sequence representation. The Concat represents a concatenation operation along the horizontal axis, and the FP represents a frame pooling operation.

develop a global and local feature extractor for gait sequences using the designed 3D basic network blocks. Huang et al. [17] explore the temporal features at three scales: frame-level, short-term and long-term. However, these methods insufficiently consider the motion differences among body parts. Therefore, some studies horizontally divide the silhouette into several parts and extract part-specific features [18,19,20,21]. Moreover, Huang et al. [22] propose 3D local operations to extract 3D volumes of body parts. Nevertheless, some irregular gait patterns (such as wearing a coat) may affect the localization accuracy and reduce the recognition accuracy.

3 Method

This section first outlines the framework of our proposed method. It then describes several components of our method, including the fine-grained part sequence learning (FPSL) module, the local motion aggregation (LMA) operation, and the weighted generalized mean (WGeM) pooling layer. Finally, it describes the loss function used to train the model.

3.1 Our Framework

Our gait recognition framework is shown in Fig. 2. Given a gait sequence \mathcal{S} of D frames, we feed \mathcal{S} into GaitFG. $\text{SF}(\cdot)$ is used to extract the shallow feature

\mathcal{F}_{sf} of \mathcal{S} , which can be formulated as:

$$\mathcal{F}_{sf} = \text{SF}(\mathcal{S}), \quad (1)$$

where $\text{SF}(\cdot)$ is implemented by two layers of 3D convolution. It then goes through two branches in parallel: a fine-grained branch and a global branch, which can be formulated as:

$$\mathcal{F}_{fb} = \text{FB}(\mathcal{F}_{sf}) \quad (2)$$

and

$$\mathcal{F}_{gb} = \text{GB}(\mathcal{F}_{sf}), \quad (3)$$

where $\text{FB}(\cdot)$ represents the fine-grained branch for extracting local features of body parts, consisting of two modules (FPSL and LMA), and $\text{GB}(\cdot)$ represents the global branch for extracting whole-body features, consisting of 3D convolution and LMA. Next, these \mathcal{F}_{fb} and \mathcal{F}_{gb} are concatenated along the horizontal axis to obtain the feature \mathcal{F}_{con} , which is mapped to the discriminative space by the frame pooling [16] operation and the WGeM pooling layer. Finally, we train the model using a combination of triplet and cross-entropy losses.

3.2 Fine-grained Part Sequence Learning Module

Horizontally slicing an input image or feature maps is typically employed to enhance the local sensitivity of gait representations [29,30,18,19]. Some recent approaches improve local adaptation by learning horizontal segmentation [20,21] or detecting semantic body parts [22]. In contrast, we perform independent spatio-temporal feature extraction from uniformly divided part sequences, thus ensuring the simplicity and generality of the model.

The FPSL module is shown in Fig. 3. Given an input feature map $\mathcal{F}_{in} \in \mathbb{R}^{C_1 \times D \times H \times W}$, where C_1 denotes the number of channels, D denotes the number of frames, H and W denote the height and width of the feature map. The input feature map is divided into k parts along the horizontal axis, which are denoted as $\mathcal{F}_{in}^j, j \in 1, 2, 3, \dots, k$, where $\mathcal{F}_{in}^j \in \mathbb{R}^{C_1 \times D \times \frac{H}{k} \times W}$. The fine-grained learning process for each part sequence is formulated as follows:

$$\mathcal{F}_{FPSL}^j = \text{3DConv}_{3 \times 3 \times 3}^{1 \times 1 \times 1}(\mathcal{F}_{in}^j), \quad (4)$$

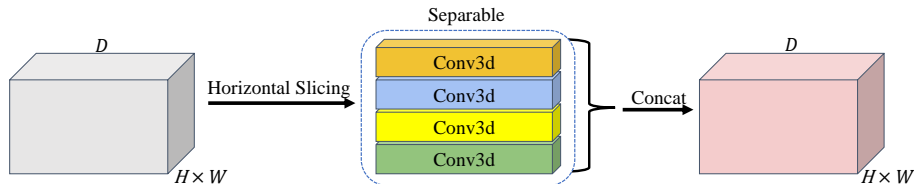


Fig. 3. Architecture of fine-grained part sequence learning module.

where $\text{3DConv}_{3 \times 3 \times 3}^{1 \times 1 \times 1}(\cdot)$ denotes a 3D convolution with a convolution kernel size of $3 \times 3 \times 3$ and a stride size of $1 \times 1 \times 1$. $\mathcal{F}_{FPSL}^j \in \mathbb{R}^{C_2 \times D \times \frac{H}{k} \times W}$ is the output of the 3D convolution operation. Note that the 3D convolution used for each part sequence is separate.

Finally, these part-based feature maps are concatenated along the horizontal axis, which can be formulated as:

$$\mathcal{F}_{FPSL} = \mathcal{F}_{FPSL}^1 \textcircled{C} \mathcal{F}_{FPSL}^2 \cdots \textcircled{C} \mathcal{F}_{FPSL}^k, \quad (5)$$

where \textcircled{C} represents the concatenation operation, $\mathcal{F}_{PFL} \in \mathbb{R}^{C_2 \times D \times H \times W}$ is the resulting feature map.

3.3 Local Motion Aggregation

It is challenging to capture discriminative motion information during sequence aggregation due to some similar frames in the sequence, especially among adjacent frames. Assume that $\mathcal{F}_m \in \mathbb{R}^{C \times D \times H \times W}$ represents the middle feature map. The LMA operation can be formulated as:

$$\mathcal{F}_{LMA} = \text{Max}_{t \times 1 \times 1}^{t \times 1 \times 1}(\mathcal{F}_m), \quad (6)$$

where $\text{Max}_{t \times 1 \times 1}^{t \times 1 \times 1}(\cdot)$ denotes a 3D max pooling operation with a kernel size of $t \times 1 \times 1$ and a stride size of $t \times 1 \times 1$. $\mathcal{F}_{LMA} \in \mathbb{R}^{C \times \frac{D}{t} \times H \times W}$ is the output of the LMA operation.

3.4 Weighted Generalized Mean Pooling

To maintain more discriminative information during spatial downsampling, we improve the GeM pooling [20] operation and propose the WGeM pooling layer (the details are shown in Fig. 4). Assume that the feature map output by the frame pooling [16] is $\mathcal{F}_{fp} \in \mathbb{R}^{C \times 1 \times 2H \times W}$, the GeM pooling operation can be formulated as:

$$\mathcal{F}_{GeM} = \left(\text{Avg}_{1 \times W}^{1 \times W} \left((\mathcal{F}_{fp})^\delta \right) \right)^{\frac{1}{\delta}}, \quad (7)$$

where $\text{Avg}_{1 \times W}^{1 \times W}(\cdot)$ represents the average pooling for a kernel size of $1 \times W$ and a stride size of $1 \times W$. The δ is a learnable parameter, which can be adaptively chosen to max or average pooling, and $\mathcal{F}_{GeM} \in \mathbb{R}^{C \times 1 \times 2H \times 1}$ is the output of the GeM. One limitation of GeM is that it treats all the elements equally. In order to keep discriminative information and suppress noise, we assign a weight to each spatial position. The weight matrix $\mathbf{E} = [\mathbf{y}_1, \mathbf{y}_2, \dots, \mathbf{y}_{2H}]^\top \in \mathbb{R}^{1 \times 1 \times 2H \times W}$ can be formulated as:

$$\mathbf{E} = \text{softmax}(\text{Conv}_{1 \times 1}^{1 \times 1}(\mathcal{F}_{fp})), \quad (8)$$

where $\text{Conv}_{1 \times 1}^{1 \times 1}$ denotes a 2D convolution operation with a convolution kernel size and stride size of 1×1 , and $\text{softmax}(\cdot)$ denotes the softmax activation function. Note that the row vectors of the weight matrix are $\mathbf{y}_h = [y_1, y_2, \dots, y_W], h \in$

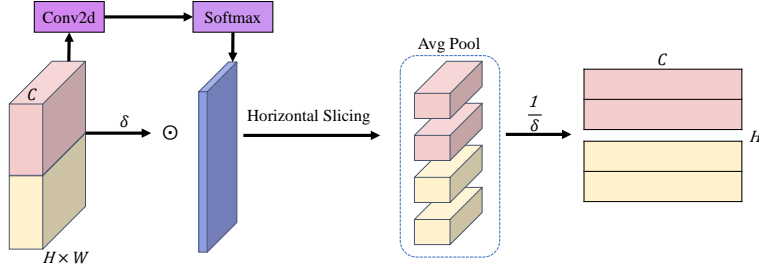


Fig. 4. Weighted generalized mean pooling layer.

$1, 2, \dots, H$, where the softmax ensures that the weighted sum of the row vectors is 1, i.e., $\sum_{j=1}^{j=W} y_j = 1$. The WGeM pooling layer can be formulated as:

$$\mathcal{F}_{WGeM} = \left(\text{Avg}_{1 \times W}^{1 \times W} \left(\mathbf{E} \odot (\mathcal{F}_{fp})^\delta \right) \right)^{\frac{1}{\delta}}, \quad (9)$$

where \odot represents the element-wise multiplication operation, and $\mathcal{F}_{WGeM} \in \mathbb{R}^{C \times 1 \times 2H \times 1}$ is the output of the WGeM.

3.5 Loss Function

In order to effectively train our model, a joint training strategy of triplet loss and cross-entropy loss is used to train the model.

The triplet loss can bring the same subjects closer and push the distance between different subjects. As shown in Fig. 2, let $\mathcal{F} \in \mathbb{R}^{C \times U}$ denote the feature following a BatchNorm layer, where U denotes the number of horizontal stripes, and the triplet loss function can be formulated as:

$$\mathbf{L}_t = \mathbf{max} [\mathbf{d}_{euc}(\mathcal{F}_a, \mathcal{F}_p) - \mathbf{d}_{euc}(\mathcal{F}_a, \mathcal{F}_g) + \beta, 0], \quad (10)$$

where the feature pair $(\mathcal{F}_a, \mathcal{F}_p)$ is selected from the same subject, the feature pair $(\mathcal{F}_a, \mathcal{F}_g)$ is selected from the different subjects, $\mathbf{d}_{euc}(\cdot, \cdot)$ is the euclidean distance function, and β is the margin of triplet loss.

In order to accelerate the network convergence and enhance the classification ability of the model, a cross-entropy loss is introduced to train the network. The feature \mathcal{F} is transformed by

$$\mathcal{F}_{logi} = \text{SeFC}(\mathcal{F}), \quad (11)$$

where $\mathcal{F}_{logi} \in \mathbb{R}^{C_{logi} \times U}$ is the output of a separated fully connected layer (SeFC), and C_{logi} represents the number of categories of training subjects. The cross-entropy loss can be formulated as:

$$\mathbf{L}_{ce} = - \sum_{c=1}^{C_{logi}} \mathbf{l}_c \log(\text{softmax}(\mathcal{F}_{logi}))_c, \quad (12)$$

Table 1. Example of a GaitFM network instantiation. The in_c and out_c represent the number of input and output channels, respectively, and the kernel means the size of the convolution kernel or pooling kernel. The * indicates that the LMA is followed by a spatial pooling [12] operation.

Network Parameter							
CASIA-B				OUMVLP			
layer	in_c	out_c	kernel	layer	in_c	out_c	kernel
Conv3d	1	32	(3,3,3)	Conv3d	1	32	(3,3,3)
Conv3d	32	32	(3,3,3)	Conv3d	32	32	(3,3,3)
Conv3d,FPSL	32	64	(3,3,3)	Conv3d,FPSL	32	64	(3,3,3)
				Conv3d,FPSL	64	64	(3,3,3)
LMA	–	–	(3,1,1)	LMA*	–	–	(3,1,1)
Conv3d,FPSL	64	128	(3,3,3)	Conv3d,FPSL	64	128	(3,3,3)
				Conv3d,FPSL	128	128	(3,3,3)
Conv3d,FPSL	128	128	(3,3,3)	Conv3d,FPSL	128	256	(3,3,3)
				Conv3d,FPSL	256	256	(3,3,3)

where \mathbf{l}_c denotes the label information of the sample represented by \mathcal{F}_{logi} , which equals 0 or 1. The final total loss function \mathbf{L}_{total} can be formulated as:

$$\mathbf{L}_{total} = \mathbf{L}_t + \mathbf{L}_{ce}, \quad (13)$$

4 Experiments

4.1 Implementation Details

Network Hyper-parameters. **1)** The FPSL module divides the feature map horizontally into k parts when extracting features, and k is set to 8. **2)** The WGeM pooling layer divides the feature map into v strips, and v is set to 128 and 64 on the CASIA-B and OUMVLP datasets, respectively. Moreover, the δ in WGeM is set to 6.5. **3)** The margin β of the triplet loss is set to 0.2.

Train Details And Test. The gait silhouettes are aligned as [31] and the silhouette images uniformly crop to a size of 64×44 . The batch size ($P \times K$) is set to (8, 8) on the CASIA-B dataset and (32, 8) on the OUMVLP dataset. During training, the number of frames D sampled per silhouette sequence is set to 30, while all frames in the sequence are fed into the network during testing. The detailed parameter settings for the network are shown in Tab. 1. When training, the model uses the adam optimizer with the initial learning rate set to 1e-4. For the CASIA-B dataset, under the ST, MT and LT settings, the number of

iterations is 80K, and the learning rate reset to $1e-4$ after 70K. For the OUMVLP dataset, the number of iterations is 160K, the learning rate reset to $1e-4$ after 150K iterations, and a label smoothing operation adds to the cross-entropy loss function.

4.2 Datasets and Evaluation Protocols

CASIA-B. The CASIA-B dataset [4] is currently the most frequently used gait dataset, containing 124 subjects. Each subject was captured in 11 camera views ($0^\circ - 180^\circ$, sampling interval 18°), each view containing six groups of normal walking (NM), two groups of walking with a bag (BG) and two groups of walking with a coat (CL), for a total of ten sequences. During the training and testing phases, experiments are conducted following the protocols in [12]: small-sample training (ST), medium-sample training (MT) and large-sample training (LT). The first 24, 62 and 74 subjects are selected as the train set for ST, MT and LT, respectively, and the remaining 100, 62 and 50 subjects as the test set. In the testing phase, the sequences (NM#01-04) are regarded as gallery, and the sequences (NM#05-06, BG#01-02 and CL#01-02) are regarded as probe for evaluation.

OUMVLP. The OUMVLP dataset [31] is one of the largest gait datasets, containing 10307 subjects. Each subject was captured at 14 camera views ($0^\circ - 90^\circ$, $180^\circ - 270^\circ$, with a sampling interval of 15°), each containing two groups of sequences at each view. Following the protocol in [12], 5153 subjects are selected for training and the remaining 5154 subjects for test. In the testing phase, the sequences (Seq#01) are regarded as gallery, while the sequences (Seq#00) are regarded as probe for evaluation.

4.3 Comparison with State-of-the-Art Methods

CASIA-B. Tab. 2 shows the performance of our proposed GaitFM with the recent state-of-the-art algorithms (including GaitSet [12], ACL [18], GaitPart [19], MT3D [16], 3D Local [22], CSTL [17], GaitGL [20], GaitMask [21]) on the CASIA-B dataset. It can be seen that our method achieves an mean view recognition accuracy of 98.0%, 95.7% and 87.9% for the NM, BG and CL walking conditions, respectively, which is 0.6%, 1.2% and 4.3% higher than GaitGL respectively, demonstrating the superiority of GaitFM in cross-view recognition. GaitFM is also quite robust to changes in walking conditions, with CSTL dropping 4.2% in accuracy from NM to BG compared to 2.3% for GaitFM and from NM to CL dropping 13.6% in accuracy compared to 10.1% for GaitFM. The robustness of GaitFM to changes in viewpoint and walking conditions is made possible by the mining of fine-grained discriminative features by the FPSL module and the adaptive aggregation of spatio-temporal information by the WGeM operation. To our knowledge, GaitFM is the first gait recognition method with a BG accuracy of 95.7% and a CL accuracy of 87.9% at 64×44 resolution. Similar

Table 2. Rank-1 accuracy (%) on CASIA-B under all views and different conditions, excluding identical-view cases.

Gallery NM #1-4		0° – 180°											
Probe		0°	18°	36°	54°	72°	90°	108°	126°	144°	162°	180°	Mean
NM #5-6	GaitSet[12]	90.8	97.9	99.4	96.9	93.6	91.7	95.0	97.8	98.9	96.8	85.8	95.0
	ACL[18]	92.0	98.5	100.0	98.9	95.7	91.5	94.5	97.7	98.4	96.7	91.9	96.0
	GaitPart[19]	94.1	98.6	99.3	98.5	94.0	92.3	95.9	98.4	99.2	97.8	90.4	96.2
	MT3D[16]	95.7	98.2	99.0	97.5	95.1	93.9	96.1	98.6	99.2	98.2	92.0	96.7
	3D Local[22]	96.0	99.0	99.5	98.9	97.1	94.2	96.3	99.0	98.8	98.5	95.2	97.5
	CSTL[17]	97.2	99.0	99.2	98.1	96.2	95.5	97.7	98.7	99.2	98.9	96.5	97.8
	GaitGL[20]	96.0	98.3	99.0	97.9	96.9	95.4	97.0	98.9	99.3	98.8	94.0	97.4
	GaitMask[21]	94.8	97.5	98.9	97.3	96.2	95.3	97.1	98.7	98.5	98.2	92.0	96.8
ours	96.8	98.4	99.2	97.9	97.0	96.9	97.9	99.4	99.4	99.3	96.1	98.0	
LT BG #1-2	GaitSet[12]	83.8	91.2	91.8	88.8	83.3	81.0	84.1	90.0	92.2	94.4	79.0	87.2
	GaitPart[19]	89.1	94.8	96.7	95.1	88.3	84.9	89.0	93.5	96.1	93.8	85.8	91.5
	MT3D[16]	91.0	85.4	97.5	94.2	92.3	86.9	91.2	95.6	97.3	96.4	86.6	93.0
	3D Local[22]	92.9	95.9	97.8	96.2	93.0	87.8	92.7	96.3	97.9	98.0	88.5	94.3
	CSTL[17]	91.7	96.5	97.0	95.4	90.9	88.0	91.5	95.8	97.0	95.5	90.3	93.6
	GaitGL[20]	92.6	96.6	96.8	95.5	93.5	89.3	92.2	96.5	98.2	96.9	91.5	94.5
	GaitMask[21]	90.7	95.2	95.9	94.1	92.5	87.2	91.6	95.2	97.4	96.7	88.5	93.2
	ours	94.5	97.2	97.9	96.6	95.3	92.2	93.7	97.3	98.2	97.8	91.7	95.7
CL #1-2	GaitSet[12]	61.4	75.4	80.7	77.3	72.1	70.1	71.5	73.5	73.5	68.4	50.0	70.4
	GaitPart[19]	70.7	85.5	86.9	83.3	77.1	72.5	76.9	82.2	83.8	80.2	66.5	78.7
	MT3D[16]	76.0	87.6	89.8	85.0	81.2	75.7	81.0	84.5	85.4	82.2	68.1	81.5
	3D Local[22]	78.2	90.2	92.0	87.1	83.0	76.8	83.1	86.6	86.8	84.1	70.9	83.7
	CSTL[17]	78.1	89.4	91.6	86.6	82.1	79.9	81.8	86.3	88.7	86.6	75.3	84.2
	GaitGL[20]	76.6	90.0	90.3	87.1	84.5	79.0	84.1	87.0	87.3	84.4	69.5	83.6
	GaitMask[21]	79.4	90.7	92.4	87.6	83.1	79.1	84.2	86.7	88.0	84.0	71.0	84.2
	ours	78.8	91.8	94.7	93.1	87.5	83.9	88.9	91.3	92.9	88.7	74.8	87.9

conclusions can also be found under ST and MT sampling strategies. Results under ST and MT are provided in the supplementary materials.

OUMVLP. Tab. 3 shows the rank-1 accuracy of our proposed GaitFM evaluated on the OUMVLP dataset compared to several current state-of-the-art algorithms, i.e., GaitSet [12], GaitPart [19], GLN [13], CSTL [17], GaitGL [20] and GaitMask [21]. The results indicate that our method outperforms the current algorithms in most views, reflecting the generalization capability of GaitFM. To be fair, our method uses the same batch size as the other two methods [20,21] that use 3D convolution. Note that the lower accuracy of our method compared to 3D Local [22] may be due to the smaller batch size of our method.

Table 3. Rank-1 accuracy (%) on OUMVLP under all views, excluding identical-view cases.

Method	Batch Size ²	Probe View														Mean
		0°	15°	30°	45°	60°	75°	90°	180°	195°	210°	225°	240°	255°	270°	
GaitSet[12]	32 × 16	79.3	87.9	90.0	90.1	88.0	88.7	87.7	81.8	86.5	89.0	89.2	87.2	87.6	86.2	87.1
GaitPart[19]	32 × 16	82.6	88.9	90.8	91.0	89.7	89.9	89.5	85.2	88.1	90.0	90.1	89.0	89.1	88.2	88.7
GLN[13]	32 × 16	83.8	90.0	91.0	91.2	90.3	90.0	89.4	85.3	89.1	90.5	90.6	89.6	89.3	88.5	89.2
CSTL[17]	32 × 8	87.1	91.0	91.5	91.8	90.6	90.8	90.6	89.4	90.2	90.5	90.7	89.8	90.0	89.4	90.2
GaitGL[20]	32 × 8	84.9	90.2	91.1	91.5	91.1	90.8	90.3	88.5	88.6	90.3	90.4	89.6	89.5	88.8	89.7
GaitMask[21]	32 × 8	86.7	90.8	91.3	91.6	91.4	91.1	90.8	89.9	89.2	90.3	90.5	90.0	89.9	89.4	90.2
Ours	32 × 8	87.2	91.2	91.5	91.7	91.5	91.1	90.9	90.1	90.0	90.6	90.8	90.2	90.0	89.6	90.5
3D Local[22]	32 × 16	86.1	91.2	92.6	92.9	92.2	91.3	91.1	86.9	90.8	92.2	92.3	91.3	91.1	90.2	90.9

4.4 Ablation Studies and Analysis

We design different ablation experiments to analyse the degree of contribution of several key components (FPSL, LMA and WGeM) of the gait recognition framework GaitFM. The ablation studies are all performed in the LT setting of the CASIA-B dataset.

Effectiveness of FPSL module. According to Tab. 4, utilising both the fine-grained and global branch improves NM by 0.8%, BG by 1.5%, and CL by 2.9% compare to using only the global branch, indicating the significant improvement in BG and CL as well as the robustness of the FPSL module to changes in appearance. In addition, the accuracy in the three walking conditions tends to improve gradually as the number of horizontal strips increases, suggesting that more strips could limit the receptive field of the network and help the network learn fine-grained discriminative features. We also replace the convolution operation of the FPSL module with a parameter-sharing convolution, and the experimental results show the effectiveness of the FPSL module in all three walking conditions.

Effectiveness of LMA module. To explore the effectiveness of the LMA aggregation sequence, we compare it with LTA [20] and spatial pooling (SP) [12], and the results are shown in Tab. 5. The aggregated sequences using LMA ($t = 3$) are 0.9% and 1.0% more accurate than the average results of LTA and SP, respectively. In the CL condition, the accuracy is improved by 1.9% compared to LTA, indicating that the LMA operation can reduce the redundant frames

² The batch size is the number of sequences contained in a batch at the training stage. For example, 32 × 16 means that a batch selects 32 subjects and each subject selects 16 sequences.

Table 4. Rank-1 accuracy at different settings of the FPSL module on CASIA-B. Part-2, Part-4 and Part-8 indicate the number of feature map bins as 2, 4 and 8 respectively. \wr denotes feature extraction using shared convolution after feature map partitioning.

Setting	Fine-grained Branch			NM	BG	CL
	Global Branch	Part-2	Part-4			
✓				97.2	94.2	85.0
			✓	97.7	94.9	86.4
✓	✓			97.5	95.1	86.9
✓		✓		97.8	95.7	87.2
✓			✓	98.0	95.7	87.9
✓			\wr	97.5	94.8	85.9

Table 5. Rank-1 accuracy under different sequence aggregation strategies on CASIA-B. SP represents a 2D max pooling operation with kernel size and stride size of 2.

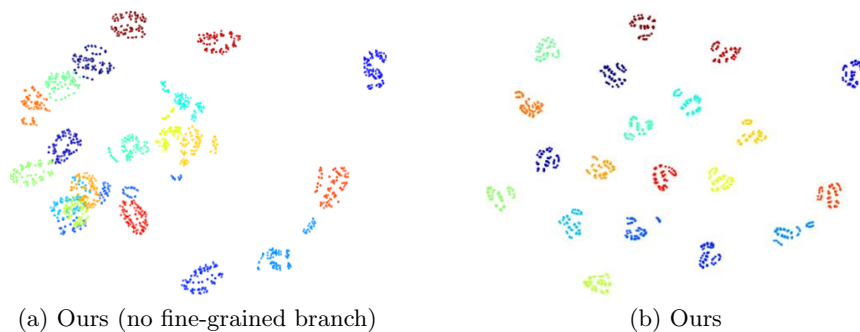
Sequence Aggregation	NM	BG	CL	Mean
SP[12]	98.0	95.2	85.4	92.9
LTA[20]	97.7	95.3	86.0	93.0
LMA($t = 3$)	98.0	95.7	87.9	93.9
LMA($t = 5$)	97.9	95.9	86.5	93.4

in local clips. We also design two groups of ablation experiments with different temporal receptive fields. The experimental results show that the mean rank-1 accuracy of the LMA ($t = 3$) operation is higher than the LMA($t = 5$), but the accuracy of LMA ($t = 5$) is 0.2 higher than that of LMA($t = 3$) in the BG condition. This may be due to the fact that subjects walk slower in the BG condition than in NM and CL, and thus a larger receptive field could facilitate the reduction of unnecessary frames in the BG sequence.

Effectiveness of WGeM. We design five groups of ablation experiments to verify the effectiveness of WGeM. The results, as shown in Tab. 6, show that the WGeM pooling layer achieves the highest accuracy in all walking conditions compared to only average pooling, max pooling or a weighted sum of them (average pooling plus max pooling or GeM pooling with adaptive parameters). In particular, the mean accuracy of WGeM pooling is 0.6% higher than that of GeM pooling, demonstrating the effectiveness of the WGeM pooling layer. It is also shown that the adaptive weight assignment mechanism further improves the adaptive aggregation spatial information capability of GeM and enhances the retention of discriminative spatial information. Furthermore, we find that

Table 6. Rank-1 accuracy under different spatial downsampling operations on CASIA-B.

Avg	Max	GeM	WGeM	NM	BG	CL	Mean
✓				96.8	94.1	83.4	91.4
✓	✓			97.7	95.3	86.0	93.0
		✓		97.8	95.6	85.2	92.9
			✓	97.8	95.3	86.7	93.3
				98.0	95.7	87.9	93.9

**Fig. 5.** Example of our method for feature visualization on the CASIA-B dataset. Different colours represent different subjects.

the mean accuracy using only max pooling or average pooling is lower than the accuracy using a weighted sum of them, indicating that both pooling operations contribute to the results.

4.5 Visualization

We randomly select 20 subjects in the CASIA-B dataset and visualize their feature distributions by t-SNE [32]. Fig. 5 shows that the separability is significantly improved with the aid of the fine-grained branch. Moreover, we also visualize the weight matrix of the WGeM, and the visualization results can be found in the supplementary materials.

5 Conclusion

This paper proposes a novel gait recognition framework, GaitFM, which integrates fine-grained and global motion properties. The PFSL module is proposed to learn part-based sequence representation. The LMA operation aggregates sequence information by compressing redundant frames. Additionally, the WGeM

pooling layer is used to improve the discriminability of spatial pooling. We perform extensive experiments on two public datasets to verify the effectiveness of GaitFM.

References

1. Singh, J.P., Jain, S., Arora, S., Singh, U.P.: Vision-based gait recognition: A survey. *Ieee Access* **6** (2018) 70497–70527
2. Yang, J., Zhou, J., Fan, D., Lv, H.: Design of intelligent recognition system based on gait recognition technology in smart transportation. *Multimedia Tools and Applications* **75** (2016) 17501–17514
3. Wang, L.: Simulation of athlete gait recognition based on spectral features and machine learning. *Journal of Intelligent & Fuzzy Systems* **40** (2021) 7459–7470
4. Yu, S., Tan, D., Tan, T.: A framework for evaluating the effect of view angle, clothing and carrying condition on gait recognition. In: 18th International Conference on Pattern Recognition (ICPR). Volume 4. (2006) 441–444
5. Yu, S., Tan, D., Tan, T.: Modelling the effect of view angle variation on appearance-based gait recognition. In: Asian Conference on Computer Vision. Volume 3851. (2006) 807–816
6. Rida, I., Almaadeed, N., Almaadeed, S.: Robust gait recognition: a comprehensive survey. *IET Biometrics* **8** (2019) 14–28
7. Uddin, M.Z., Muramatsu, D., Takemura, N., Ahad, M.A.R., Yagi, Y.: Spatio-temporal silhouette sequence reconstruction for gait recognition against occlusion. *IPSN Transactions on Computer Vision and Applications* **11** (2019) 1–18
8. Yeoh, T., Aguirre, H.E., Tanaka, K.: Clothing-invariant gait recognition using convolutional neural network. In: 2016 International Symposium on Intelligent Signal Processing and Communication Systems (ISPACS). (2016) 1–5
9. Yao, L., Kusakunniran, W., Wu, Q., Xu, J., Zhang, J.: Collaborative feature learning for gait recognition under cloth changes. *IEEE Transactions on Circuits and Systems for Video Technology* **32** (2021) 3615–3629
10. Shiraga, K., Makihara, Y., Muramatsu, D., Echigo, T., Yagi, Y.: Geinet: View-invariant gait recognition using a convolutional neural network. In: 2016 international conference on biometrics (ICB). (2016) 1–8
11. Li, X., Makihara, Y., Xu, C., Yagi, Y., Ren, M.: Gait recognition via semi-supervised disentangled representation learning to identity and covariate features. In: Proceedings of the IEEE/CVF Conference on Computer Vision and Pattern Recognition (CVPR). (2020) 13309–13319
12. Chao, H., Wang, K., He, Y., Zhang, J., Feng, J.: Gaitset: Cross-view gait recognition through utilizing gait as a deep set. *IEEE Transactions on Pattern Analysis and Machine Intelligence* **44** (2021) 3467–3478
13. Hou, S., Cao, C., Liu, X., Huang, Y.: Gait lateral network: Learning discriminative and compact representations for gait recognition. In: European Conference on Computer Vision (ECCV). (2020) 382–398
14. Hou, S., Liu, X., Cao, C., Huang, Y.: Set residual network for silhouette-based gait recognition. *IEEE Transactions on Biometrics, Behavior, and Identity Science* **3** (2021) 384–393
15. Hou, S., Liu, X., Cao, C., Huang, Y.: Gait quality aware network: Toward the interpretability of silhouette-based gait recognition. *IEEE Transactions on Neural Networks and Learning Systems* (2022)
16. Lin, B., Zhang, S., Bao, F.: Gait recognition with multiple-temporal-scale 3d convolutional neural network. In: Proceedings of the 28th ACM International conference on Multimedia. (2020) 3054–3062
17. Huang, X., Zhu, D., Wang, H., Wang, X., Yang, B., He, B., Liu, W., Feng, B.: Context-sensitive temporal feature learning for gait recognition. In: Proceedings

- of the IEEE/CVF International Conference on Computer Vision (ICCV). (2021) 12909–12918
18. Zhang, Y., Huang, Y., Yu, S., Wang, L.: Cross-view gait recognition by discriminative feature learning. *IEEE Transactions on Image Processing* **29** (2019) 1001–1015
 19. Fan, C., Peng, Y., Cao, C., Liu, X., Hou, S., Chi, J., Huang, Y., Li, Q., He, Z.: Gaitpart: Temporal part-based model for gait recognition. In: *Proceedings of the IEEE/CVF conference on computer vision and pattern recognition (CVPR)*. (2020) 14225–14233
 20. Lin, B., Zhang, S., Yu, X.: Gait recognition via effective global-local feature representation and local temporal aggregation. In: *Proceedings of the IEEE/CVF International Conference on Computer Vision (ICCV)*. (2021) 14648–14656
 21. Lin, B., Liu, Y., Zhang, S.: Gaitmask: Mask-based model for gait recognition. In: *32nd British Machine Vision Conference (BMVC)*. (2021) 363
 22. Huang, Z., Xue, D., Shen, X., Tian, X., Li, H., Huang, J., Hua, X.S.: 3d local convolutional neural networks for gait recognition. In: *Proceedings of the IEEE/CVF International Conference on Computer Vision (ICCV)*. (2021) 14920–14929
 23. Zhang, Y., Huang, Y., Wang, L., Yu, S.: A comprehensive study on gait biometrics using a joint cnn-based method. *Pattern Recognition* **93** (2019) 228–236
 24. Sepas-Moghaddam, A., Ghorbani, S., Troje, N.F., Etemad, A.: Gait recognition using multi-scale partial representation transformation with capsules. In: *2020 25th International Conference on Pattern Recognition (ICPR)*. (2021) 8045–8052
 25. Han, J., Bhanu, B.: Individual recognition using gait energy image. *IEEE transactions on pattern analysis and machine intelligence* **28** (2005) 316–322
 26. Liao, R., Yu, S., An, W., Huang, Y.: A model-based gait recognition method with body pose and human prior knowledge. *Pattern Recognition* **98** (2020) 107069
 27. An, W., Yu, S., Makihara, Y., Wu, X., Xu, C., Yu, Y., Liao, R., Yagi, Y.: Performance evaluation of model-based gait on multi-view very large population database with pose sequences. *IEEE transactions on biometrics, behavior, and identity science* **2** (2020) 421–430
 28. Li, X., Makihara, Y., Xu, C., Yagi, Y., Yu, S., Ren, M.: End-to-end model-based gait recognition. In: *Proceedings of the Asian conference on computer vision (ACCV)*. (2020) 3–20
 29. Sun, Y., Zheng, L., Yang, Y., Tian, Q., Wang, S.: Beyond part models: Person retrieval with refined part pooling (and a strong convolutional baseline). In: *Proceedings of the European conference on computer vision (ECCV)*. (2018) 480–496
 30. Fu, Y., Wei, Y., Zhou, Y., Shi, H., Huang, G., Wang, X., Yao, Z., Huang, T.: Horizontal pyramid matching for person re-identification. In: *Proceedings of the AAAI conference on artificial intelligence (AAAI)*. (2019) 8295–8302
 31. Takemura, N., Makihara, Y., Muramatsu, D., Echigo, T., Yagi, Y.: Multi-view large population gait dataset and its performance evaluation for cross-view gait recognition. *Ipsj Transactions on Computer Vision and Applications* **10** (2018) 1–14
 32. Van der Maaten, L., Hinton, G.: Visualizing data using t-sne. *Journal of machine learning research* **9** (2008)